

Ensemble numerical forecasts of the sporadic Kuroshio water intrusion (kyucho) into shelf and coastal waters

Atsuhiko Isobe · Shin'ichiro Kako · Xinyu Guo ·
Hidetaka Takeoka

Received: 31 August 2011 / Accepted: 27 December 2011 / Published online: 17 January 2012
© The Author(s) 2012. This article is published with open access at Springerlink.com

Abstract The finite volume coastal ocean model downscaling ocean reanalysis and forecast data provided by the Japan Coastal Ocean Predictability Experiment (JCOPE2) are used to forecast sudden Kuroshio water intrusion events (kyucho) induced by frontal waves amplified south of the Bungo Channel in 2010. Two-month hindcast computations give initial conditions of the following 3-month forecasts computations which consist of ten ensemble members. The temperature time series computed by these ten members are averaged to compare with that actually observed in the Bungo Channel, where sudden temperature rises related to kyucho events are remarkable in February, August, and September. Overall, the intense kyucho events actually observed in these months are predicted successfully. However, intense kyucho events are forecasted frequently during the period of May through June even though intense kyucho events are absent during this period in the actual ocean. It is suggested that the present downscaling forecast model requires reliable lateral boundary conditions provided by JCOPE2 data to which numerous Argo data are assimilated to enhance the accuracy. In addition, it seems likely that the model accuracy is reduced by small eddies moving along the shelf break.

Keywords JCOPE2 · FVCOM · Ensemble forecast · Kyucho · Argo

Responsible Editor: Tal Ezer

This article is part of the Topical Collection on the *3rd International Workshop on Modelling the Ocean 2011*

A. Isobe (✉) · S. Kako · X. Guo · H. Takeoka
Center for Marine Environmental Studies, Ehime University,
2-5 Bunkyo-cho,
Matsuyama 790-8577, Japan
e-mail: aisobe@ehime-u.ac.jp

1 Introduction

Western boundary currents such as the Kuroshio in the North Pacific are always accompanied by frontal waves on the onshore side. Unlike the Gulf Stream in the North Atlantic, the Kuroshio path is located very close to the western boundary (the southern coast of Japan in this case), so the frontal waves excited along the ocean currents frequently extend onto the shallow shelf and coastal waters (Akiyama and Saitoh 1993; Arai 2005) and rapidly alter the marine environment in these areas (Koizumi and Kohno 1994; Katano et al. 2007; Hirose et al. 2008). In fact, it has been reported that these frontal waves amplified at the shelf break cause sporadic Kuroshio water intrusion into various coastal waters south of Japan, where cultured fishes and fixed nets have been frequently damaged by sudden increases in both temperature and current speed associated with this warm water intrusion (Takeoka and Yoshimura 1988 and references therein). The Japanese term “kyucho” (meaning sudden stormy currents) has been used by the oceanographic community of Japan as well as fishermen to refer to these intrusion events, which have heretofore received attention from oceanographers (e.g., Uda 1953). Besides the disadvantages to inshore fisheries as mentioned above, kyucho events have an advantage in that catches of commercially high-valued fishes increase suddenly in coastal waters during these events, presumably because fish around shelf breaks avoid rapid temperature changes (Hashida 2011, personal communication). Thus, a research project in high demand is to establish kyucho forecasting similar to weather forecasting.

To date, it has been difficult to forecast ocean currents and hydrographic properties in shelf and coastal waters despite the development of high-performance computers such as the Earth Simulator (Masumoto et al. 2004) along

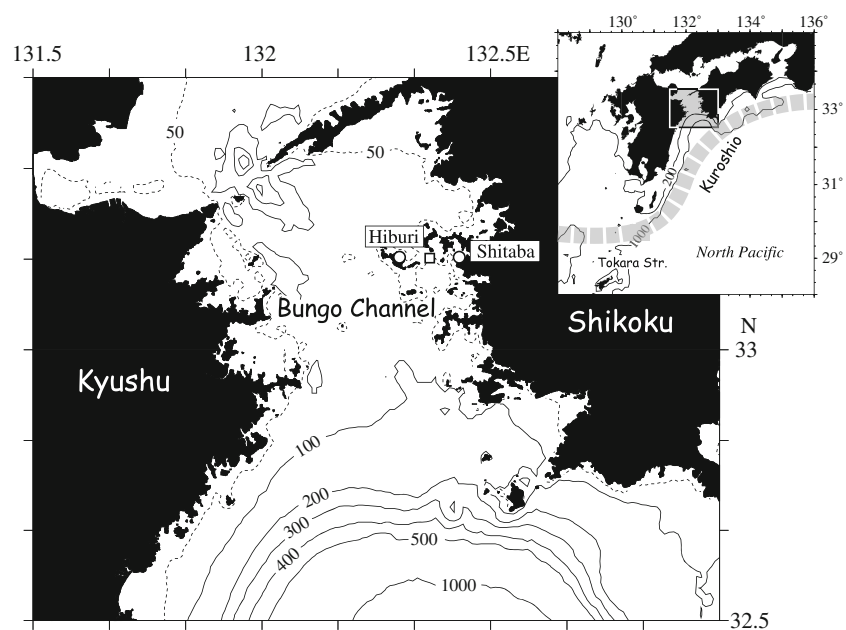
with sophisticated numerical model codes. The development of numerical forecasting in these shallow waters seems to have been prevented by two obstacles. One is that the density of observation stations is too sparse to construct objectively analyzed datasets suitable for providing reliable initial conditions for models. For instance, one of the most powerful tools to obtain spatiotemporally dense oceanographic data is satellite altimetry, which provides sea surface height (SSH) data approximately once every 10 days with spatial resolution of 100 km, while both temporal and spatial scales required for resolving Kuroshio frontal waves are one order of magnitude smaller (see Table 1 in James et al. 1999). The other obstacle is uncertain in lateral boundary conditions. Even if a forecast model does a reasonable job of simulating ocean currents within the model domain, a wrong condition at lateral boundaries may reduce model accuracy.

In the present study, special attention is given to kyucho events in the Bungo Channel (Fig. 1), the width and axis length of which are both approximately 50 km. In spite of the above two limitations, the present attempt to forecast kyucho events may succeed because more oceanic data have recently become available to the oceanographic community. Apparently, it is not yet possible to overcome the former obstacle because we have no way of providing gridded oceanic data (e.g., SSH) operationally once a day with the several kilometers resolution required for kyucho forecasts in the relatively narrow Bungo Channel. However, daily ocean reanalysis and forecast data provided by the Japan Coastal Ocean Predictability Experiment (JCOPE2; Miyazawa et al. 2008, 2009) allow us to impose reliable lateral boundary conditions on numerical coastal models.

It is difficult to detect kyucho events directly in JCOPE2 data because their horizontal resolution of 1/12 of a degree is unlikely to resolve Kuroshio frontal waves accurately (Isobe et al. 2004). Probably the simplest way to simulate kyucho events is to downscale JCOPE2 data using a numerical model suitable for reproducing small-scale features in shelf and coastal waters. The present study employs the finite volume coastal ocean model (FVCOM; Chen et al. 2003) for resolving complex topography in shallow waters using triangular cell grids. In fact, a hindcast computation using JCOPE2 data as boundary conditions of the FVCOM well reproduces the kyucho events in 2003 (Isobe et al. 2010) because mesoscale warm eddies impinging on the Kuroshio south of Japan trigger the kyucho occurrence and these eddies are well reproduced in the JCOPE2 analysis. In addition, the JCOPE2 model successfully forecasts Kuroshio meanders after removing the assimilation schemes incorporated into the model (Miyazawa et al. 2005), and FVCOM computations using JCOPE2 forecast data as lateral boundary conditions are therefore expected to forecast kyucho events as they occur in the actual ocean.

The objective of the present study is to examine the capability of ensemble kyucho forecasts by downscaling either physical processes or resolution in JCOPE2 analysis into a smaller FVCOM domain (i.e., one-way nested model) around the Bungo Channel. In the present application, 3-month forecast computations follow 2-month hindcast computations, during which observation data are not assimilated into the FVCOM domain. This is because, as mentioned above, the fine structure of Kuroshio frontal waves is likely to be destroyed by assimilating sporadic observations insufficient

Fig. 1 Study area. The area within the shaded square in the upper right inset map is enlarged in the lower left panel. The Kuroshio path is shown schematically on the inset map. Also shown are isobaths in meters. Temperature at 5-m depth below the sea surface is observed at two stations (Shitaba and Hiburi) denoted by open circles. The forecast temperature at the open square is compared with the temperature averaged between the two stations



for coastal waters. The insufficient accuracy that may appear in the present forecast computations is caused by the uncertainty of small-scale processes generated in the FVCOM domain as well as that included within JCOPE2 data. It is worthwhile to specify causes reducing the capability of the forecasts to improve this “first generation” of kyucho forecast models.

2 Data and methods

2.1 Kyucho events in the Bungo Channel

Experiments are conducted to forecast the kyucho events observed in 2010 in the Bungo Channel. Before describing the experimental details, we next present a temperature record in which several kyucho events are observed (Fig. 2). This time series is the average of those observed 5 m below the sea surface at Hiburi and Shitaba stations (Fig. 1) because each single temperature record was occasionally interrupted by mechanical errors. The temperature record band-passed between 5 days and 1 year indicates that intense kyucho events occur during two periods as shown by the shading in Fig. 2. First, there are temperature increases of more than 3°C even in the midwinter, although in general, warm water is prevented from intruding onto

shallow shelves because the intense winter cooling makes shallow waters vertically well-mixed. It is therefore suggested that highly suitable conditions for triggering the kyucho occurrence are established during this period. Frequent relatively weak temperature rises are revealed during the period May through June. However, it should be noted that kyucho events comparable to those in the first period occur in the midsummer and that the temperature rises by about 3°C twice during the period July through September.

Isobe et al. (2010) point out that the kyucho events in midsummer 2003 in the Bungo Channel were triggered by mesoscale warm eddies impinging on the Kuroshio south of the channel. Indeed, the SSH maps on days *a*, *b*, and *c* (Fig. 2) demonstrate that the sharpness of the Kuroshio front increases gradually (lower three panels in Fig. 3) as the areas with high SSH anomalies extend westward (upper three panels in Fig. 3). It is anticipated that kyucho events (i.e., development of Kuroshio frontal waves) are likely to occur on day *c* because the frontal sharpness is a condition favorable for the enhancement of baroclinic instability.

2.2 Model setup and nests

We next describe details of the numerical model used for hindcast computations. The behavior of mesoscale warm eddies is well reproduced in JCOPE2 reanalysis in which datasets derived from both satellites and the Global Temperature Salinity Profile Program (GTSP) including Argo data are assimilated (Miyazawa et al. 2008, 2009). Hence, it is anticipated that downscaling these reanalysis data to data for shelf and coastal waters will allow us to reproduce the condition favoring kyucho events. The SSH, temperature, salinity, and horizontal components of currents in the JCOPE2 reanalysis data are given to the lateral boundaries of the FVCOM domain (Fig. 4), where the length of cell edges is the same as that of JCOPE2 data (1/12°) at open boundaries so that the FVCOM is connected to JCOPE2 data without spatial interpolations of variables. Thereby, this one-way nested model is likely to conserve volume transport between two different models. This is a clear advantage of unstructured grid models like the FVCOM over models with a uniform grid in constructing nested models. The length in the channel reduces to less than 1 km, which is sufficiently small to reproduce both frontal waves and complex topography (see the enlarged panel of Fig. 4). Sidewall boundaries are imposed at Hayasui Strait and Awaji Island because the throughflow that may alter circulation in the model domain is unclear around these narrow straits (~10 km width) (Chang et al. 2009) and because there is no way of knowing current and hydrographic conditions in these straits during the course of the hindcast/forecast computations; note that the JCOPE2 analysis does not provide us with oceanic conditions within the shallow Seto Inland Sea.

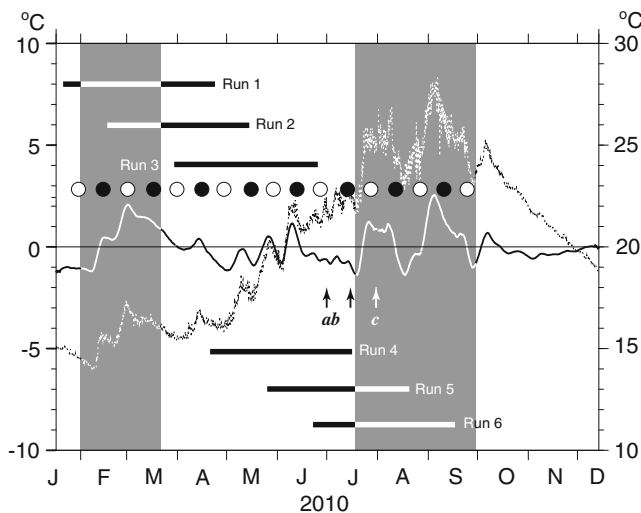
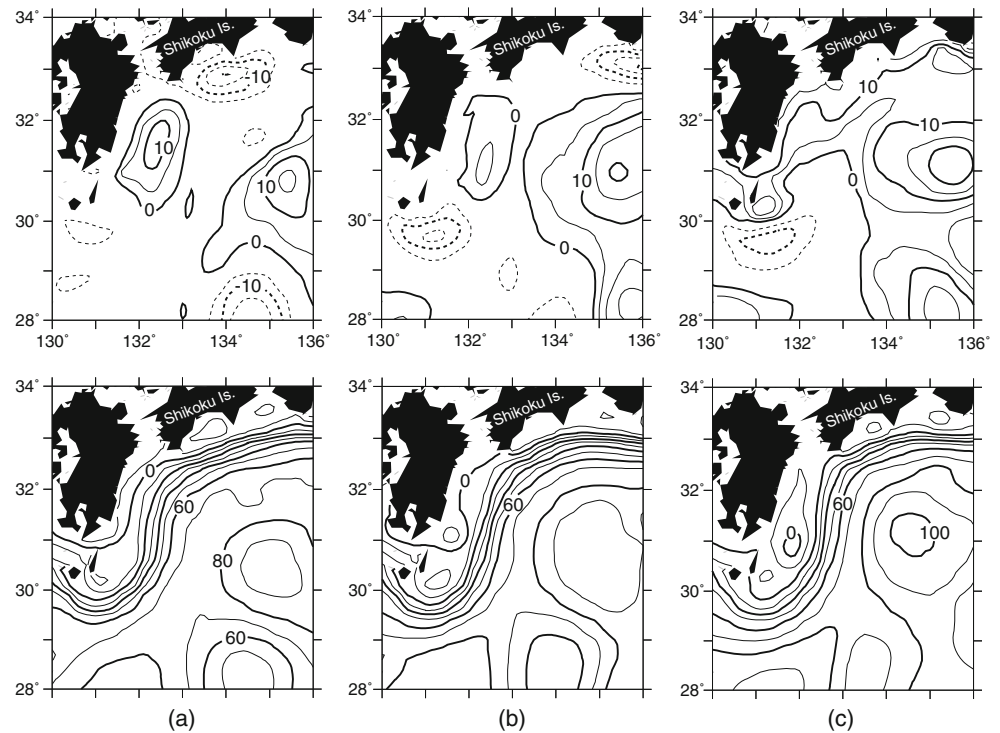


Fig. 2 Observed temperature record. The *dotted curve* indicates temperature averaged between two observation stations (Fig. 1). The observed temperature anomaly from the annual average is low-passed using a 5-day box-car filter, and the annual variation is removed by fitting a sinusoidal curve with a least square method (*solid curve*). See the right ordinate for the raw temperature record and left ordinate for the processed record. The *bars* show the periods of forecast runs. *Two shaded bands* emphasize the intense kyucho occurrences during February, August, and September. SSH maps derived from JCOPE2 reanalysis data at the points labeled *a*, *b*, and *c* are depicted in Fig. 3. The *closed and open circles* indicate new and full moons, respectively

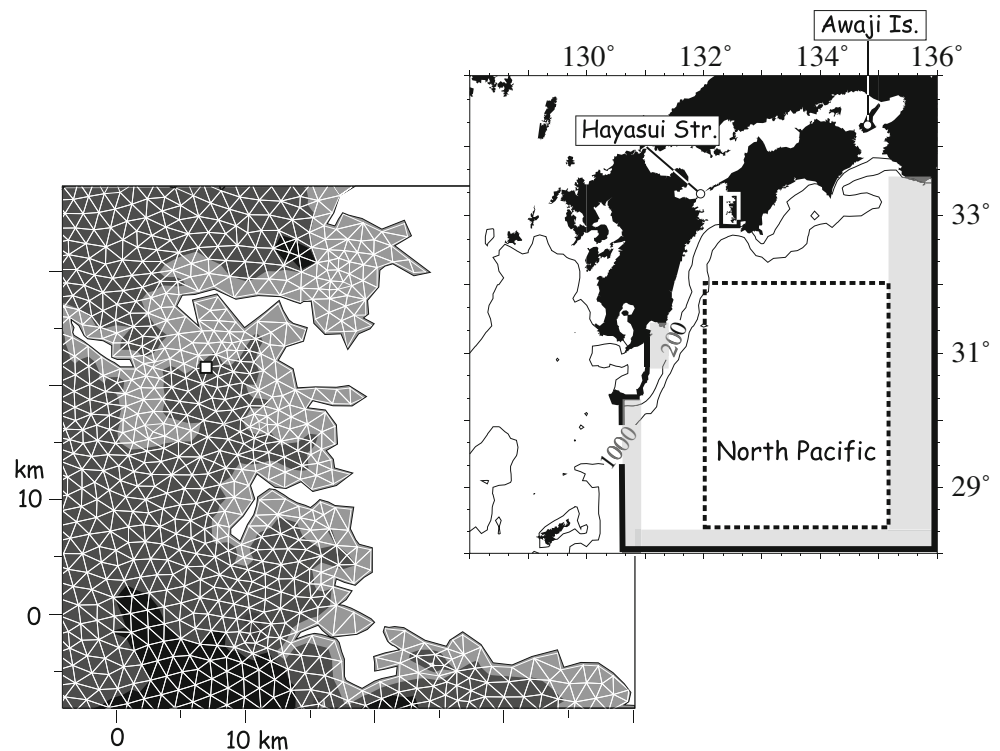
Fig. 3 SSH anomalies (*upper panels*) and SSH (*lower*) at *a*, *b*, and *c* in Fig. 2. The anomalies are computed by removing the SSH averaged over the period *a* through *c*. The contour interval is 5 (10) cm in the *upper* (*lower*) panels



Perturbations generated by connecting two different models are removed in sponge regions (shading in Fig. 4), where all modeled variables are restored to JCOPE2 reanalysis data. The coefficient (a reciprocal of time) of restoring terms diminishes linearly from $1/6 \text{ h}^{-1}$ at the lateral boundaries to zero at the inner edge of the sponge regions. The width of the

sponge regions is doubled along the eastern boundary to carefully retain the shape of warm eddies propagating westward as baroclinic Rossby waves and/or advection due to the Kuroshio Countercurrent. The FVCOM domain is divided into 23 layers vertically, and 23-layer JCOPE2 data are interpolated linearly to each FVCOM layer in the sponge regions.

Fig. 4 Area modeled using the FVCOM. The *bold lines in the upper right panel* denote the lateral boundaries of the FVCOM domain. *Shading in the upper right panel* indicates “sponge layers” in which FVCOM results are restored to JCOPE2 data to remove artificial disturbances caused by the connection between two different model results. Argo data within the box outlined by the *bold broken line* are used for the computation in Table 1. Also shown are 200- and 1,000-m isobaths. The area within the *small rectangle in the upper right panel* is enlarged in the *lower left panel* to illustrate unstructured triangular cell grids and depths represented by *thin white lines and shading*, respectively. *Light shading* is used for areas shallower than 50 m, while areas deeper than 100 m are represented by *dark shading*



Two datasets are combined to give depth data to each triangular cell grid of the FVCOM. The topographic dataset with 1/12° resolution (ETOPO5) provided by the US National Geophysical Data Center is used for the area south of 31.5° N, while the 500-m gridded topographic dataset provided by the Marine Information Research Center, Japan is used for the area north of 31° N. The above two topographic datasets are blended using a coefficient varying linearly in space between 31° N and 31.5° N latitudes. The depth in each triangular cell grid is determined by interpolating the nearest 16 topographic data weighted by the inverse distance.

The procedures for hindcast computations are shown in Fig. 5. Daily JCOPE2 reanalysis data are imposed at the lateral boundaries through linear interpolation at each time step. To date, no research project has pointed out that kyucho occurrences in the Bungo Channel are triggered by momentum and heat fluxes through the sea surface. Nevertheless, winter northerly monsoon winds (hence, intense cooling) are likely to prevent warm Kuroshio water from intruding northward on the shelf. Thus, in the present application, monthly averaged wind stresses and sea surface temperature (SST) are imposed over the FVCOM domain. In addition, daily wind stresses are imposed over the model domain for comparison. In lieu of adopting the Quick Scatterometer (QSCAT) winds unavailable at this time, we employ the monthly averaged wind vectors observed by the Advanced Scatterometer (ASCAT) after gridding with an optimal interpolation method (Kako et al. 2011). The drag coefficient of Large and Pond (1981) is adopted to convert wind speeds into stresses. SST over the FVCOM domain is restored to SST provided by climatologically averaged monthly JCOPE2 data on a time scale of 5 days. It is reported that kyucho events in the Bungo Channel tend to generate at neap tides because of weak vertical mixing (Takeoka et al. 1993). It is, however, ambiguous that the kyucho occurrences in 2010 are synchronized with fortnightly neaps–springs cycles (Fig. 2) and so tidal forcing is not applied to the present model. Hindcast computations are started with initial conditions produced using JCOPE2 data and are thereafter continued over the course of 2 months, which is sufficient for initial disturbances to spin-down over the model

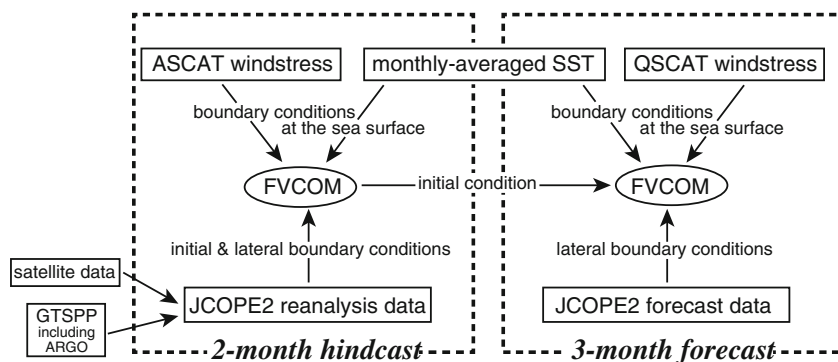
domain and for small-scale features (say, frontal waves) not resolved in the JCOPE2 reanalysis to be generated in the FVCOM.

2.3 Procedures of forecast computations

Three-month forecasts follow the above hindcasts, with the results at the end of the computations used as initial conditions (Fig. 5). Three-month period is chosen as the forecast duration because JCOPE2 provides us with 3-month daily forecast data, which are set to lateral boundaries in the same manner as in the hindcast computations. In addition, modeled SST is restored to monthly averaged JCOPE2 forecast data on a timescale of 5 days so that small-scale features revealed in the SST field of the original JCOPE2 analysis do not destroy those in the FVCOM domain. Forecast winds such as those of the Numerical Analysis and Prediction System of the Japan Meteorological Agency are not used to drive the present forecast model because, as mentioned above, short-term wind fluctuations are not critical to kyucho occurrences and because the use of forecast winds complicates interpretations of the forecast accuracy. Monthly averaged wind stresses computed using QSCAT data in the period 2002 through 2008 drive the model domain during the course of the forecast computations. Tidal forcing is not included in the forecast computations as in the hindcast computations.

The forecast computations are conducted six times for 2010 (bars in Fig. 2) as follows: Each forecast run consists of ten ensemble members; ten temperature records at the midpoint between Shitaba and Hiburi (box in Fig. 1) are averaged to compare with the observed time series in Fig. 2. The computations of ten ensemble members are started from different perturbed initial states generated by the breeding method (Toth and Kalnay 1993) as schematically shown in Fig. 6. In the first run (referred to as run 1), random temperature perturbations with a standard deviation of 0.1°C are added to the temperature field in the 2-month hindcast computation on 21 January. Ten perturbation patterns provide us with ten different forecast members (solid circles in

Fig. 5 Flowchart describing the relationship between hindcast/forecast computations and dataset input to the models



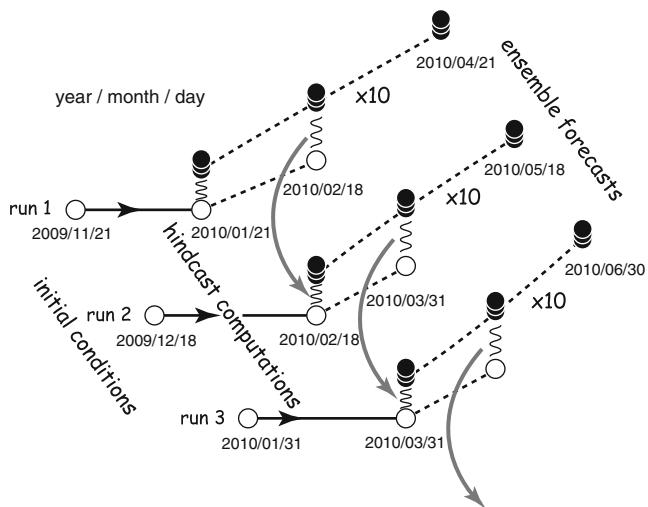


Fig. 6 Schematic view of the breeding method. See text for details

Fig. 6) in the following 3 months. Simultaneously, a single “unperturbed” ensemble member without the addition of initial perturbations is computed until the beginning of run 2 (open circle with the broken line at run 1). The temperature differences between perturbed and unperturbed ensemble members on 18 February are normalized so that their standard deviations are adjusted to 0.1°C in each combination and are added as the initial perturbations to the next ten ensemble members of run 2. In the same manner as for run 2, four sets of hindcast and forecast runs (runs 3–6) are thereafter repeated as shown by the bars in Fig. 2. Overall, the coefficients of correlation among normalized standard deviations of each ensemble member are very small (~ 0.2).

3 Results

We first show the results for run 1 which give us confidence in forecasting kyuchō events in the Bungo Channel. To emphasize the timing of the kyuchō occurrence, Fig. 7 graphs de-trended time series of temperature anomalies at the box position in Fig. 1. Thin curves indicating ten ensemble members show that temperature rises suddenly in mid-February in spite of stochastic fluctuations considerably differing for each member; see the solid curve at the base of the figure for the standard deviation of ensemble members from the averaged curve. The temperature rise in the actual ocean is observed over the course of February (see the broken curve in Fig. 7), while the average (bold curve) of ten members shows that the onset of the temperature rise seems to be delayed by about a week. Nevertheless, we emphasize that the kyuchō occurrence in February 2010 is forecasted successfully in run 1 conducted about 20 days previously.

Both satellite-observed and forecast SST maps demonstrate that the kyuchō event occurs in mid-February when the Kuroshio front approaches the Bungo Channel (Fig. 8). A cloud-free image taken on 20 February 2010 (images before and after the 20th were unavailable owing to cloud) and downloaded from the website of the North Pacific Region Environmental Cooperation Center (<http://www.npec.or.jp/>) shows that the Kuroshio front with temperature between 16.5°C and 18.5°C is embedded on the shelf of the Bungo Channel mouth and that warm water originating from the Kuroshio extends further to the north in the channel. The SST maps forecasted every 5 days also represent both the Kuroshio front located close to the channel and northward extension of warm water in mid-February. However, SST is higher than that observed by the satellite partly because the sea surface cooling within the narrow channel is incorporated by restoring SST computed using the relatively coarse JCOPE2 model.

The present downscaling model was capable of forecasting kyuchō events if the accuracy in Fig. 7 was maintained throughout all forecast runs. It should, however, be noted that the accuracy considerably differs for each forecast run (Fig. 9). For instance, intense kyuchō events rarely occur in the period April through June in the actual ocean (Fig. 2), although remarkable kyuchō events frequently appear in

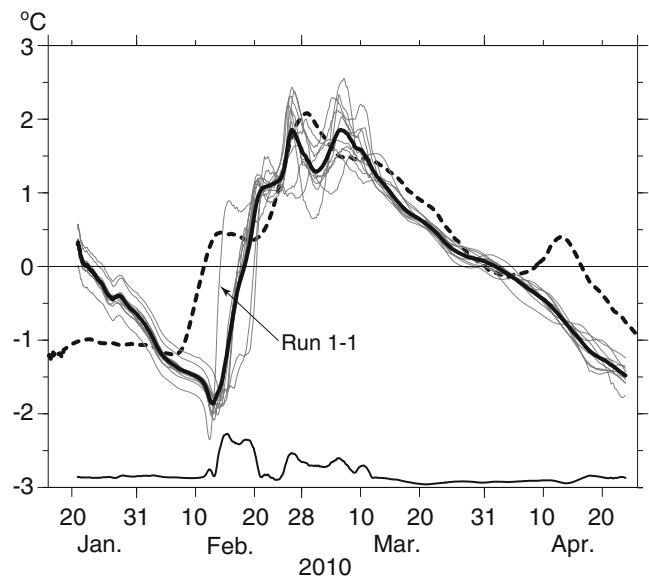


Fig. 7 Time series of temperature anomalies in the period of run 1. The observed series (*broken curve*) is the same as the solid curve in Fig. 2 except for de-trending in lieu of removing the annual variation because of the 3-month computation. The temperature records forecast by ten ensemble members are denoted by *thin solid curves*; the curve of the first member is indicated by the *arrow*. The *bold solid curve* shows the time series averaged for the ten ensemble members. The standard deviation of ensemble members (*thin solid curves*) from the averaged value (*bold curve*) is indicated by the *solid curve at the bottom of the figure*

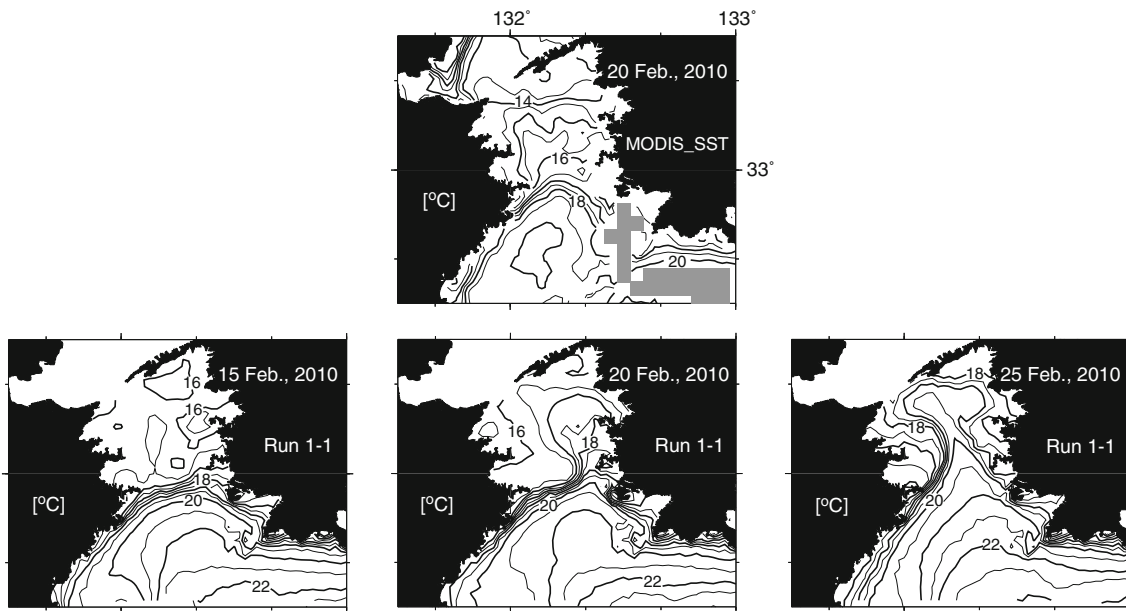
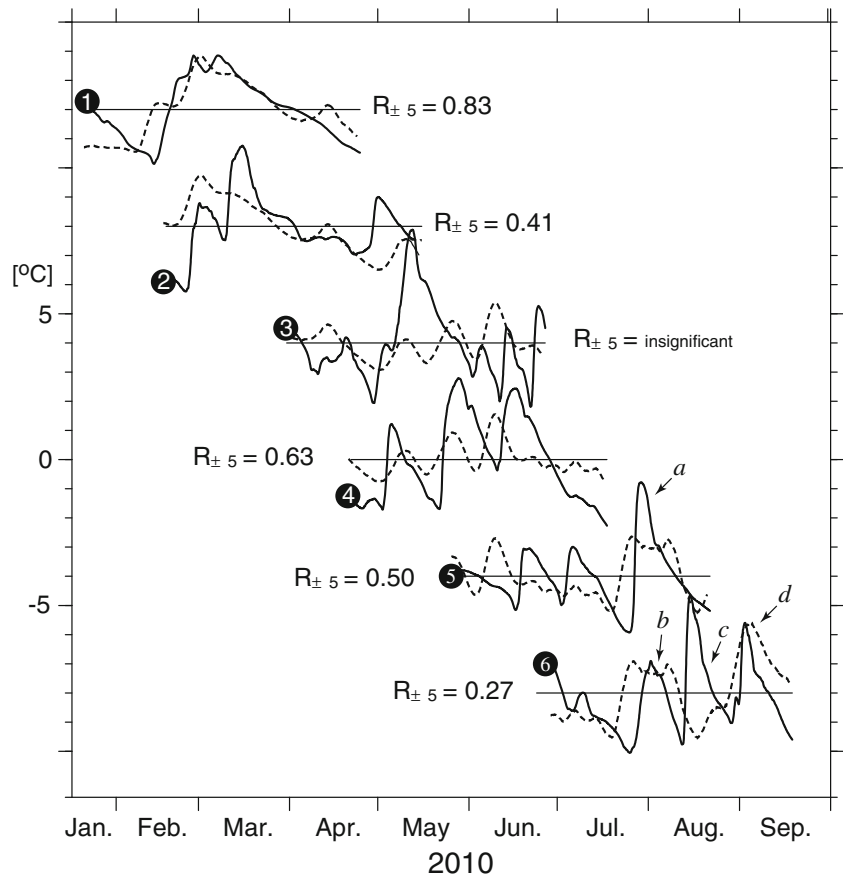


Fig. 8 SST maps during the period of run 1. The satellite-derived SST is shown in the upper panel. Shading indicates areas covered by clouds. The lower three panels show SST maps computed for the first member of run 1. The contour interval is 0.5°C in both upper and lower panels

runs 3 and 4 (Fig. 9). Sudden temperature rises in run 5 (see the arrow with the letter *a*) and run 6 (arrows with the letters *b* and *d*) are well forecasted in the present model, while a

temperature rise in run 6 (the arrow with the letter *c*) does not occur in the actual ocean. The numerals in each graph are the maximum values of the lag-correlation coefficient

Fig. 9 Comparison between observed (broken curves) and forecast (solid curves) temperature records. The forecast records are the average for ten ensemble members. Both time series are low-passed by a 5-day box-car filter and are de-trended during the forecast period of each run. The curves indicate anomalies from the temporally averaged value during the forecast period. The solid circles with numerals are plotted at the beginning of each forecast run. Each curve is shifted downward by 2.5°C for ease of presentation. See the text for the meaning of the letters *a* to *d*. The numerals for each graph indicate the maximum values of the lag-correlation coefficient within ±5 days. The coefficients are all insignificant over the course of 10 days in run 3, according to a *t* test with a 95% confidence level



within ± 5 days to roughly show the similarity between the forecast and observed time series.

4 Discussion

4.1 Reliability of the lateral boundary conditions

As mentioned above, the kyucho events actually observed during the two shaded periods in Fig. 2 are all forecasted (mid-February and *a* (*b*) and *d* in Fig. 9) in the present experiment, while the kyucho events revealed in the forecast computations are not always observed in the actual ocean (run 3, run 4, and *c*). In general, the accuracy of downscaling computations depends strongly on the reliability of lateral boundary conditions, and it is thus worth investigating to what extent the boundary conditions provided by JCOPE2 data are reliable. The number of Argo floats south of Japan is likely to be crucial to enhancing the reliability of JCOPE2 data because hydrographic data assimilated to the reanalysis model are derived from numerous Argo floats and because the number of Argo floats carried passively by ocean currents is unlikely to be stable south of Japan.

We first seek areas correlated significantly with the lateral boundaries of the forecast computations and thereafter investigate the number of Argo floats passing these areas in the past. The lag-correlation maps of SSH at the lateral open boundaries are depicted using JCOPE2 reanalysis data in which the satellite-derived SSH is assimilated (Fig. 10). Two representative locations at the mid-points of the eastern and southern boundaries are chosen for the computation because these boundaries are located “upstream” of westward-propagating mesoscale eddies that trigger the kyucho occurrence in the Bungo Channel. The significant correlation areas are traceable roughly in the past 5 months (bold curves in Fig. 10), suggesting that the reliability of the lateral boundary conditions depends on whether or not eddies moving around these areas are reproduced appropriately in JCOPE2 data.

The number of Argo floats within the shaded areas of Fig. 10 during the past 5 months is next counted in the course of each 3-month forecast run (Fig. 11). We here use the Argo dataset arranged by Oka et al. (2007; <http://ocg.aori.u-tokyo.ac.jp/member/eoka/data/NPargodata/>). Note that the float number should decrease monotonically in the figure because the period during which Argo data are not assimilated increases gradually as the 3-month forecast computations proceed. For instance, open boundary conditions (i.e., JCOPE2 analysis) on day 0 of each forecast run undergo the assimilation of Argo data over the course of the past 5 months, while the conditions on day 90 undergo the assimilation only in 2 months of the past 5 months. It should

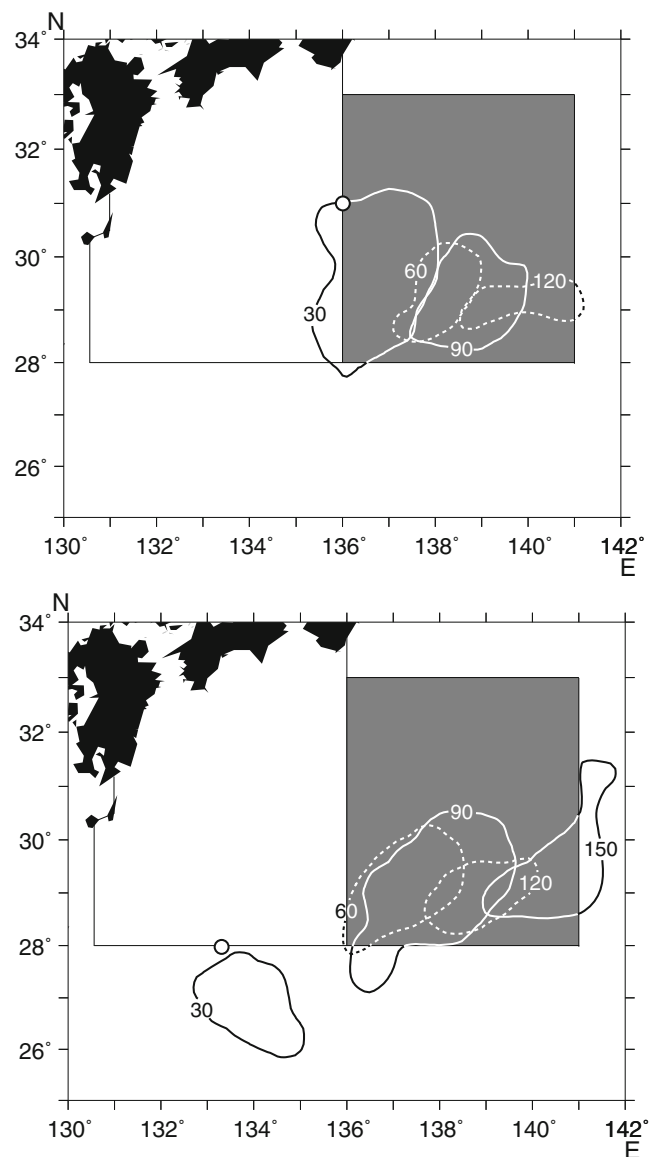


Fig. 10 Lag-correlation maps of SSH at locations denoted by *open circles*. The areas with statistically significant correlation coefficients according to a *t* test with a 99% confidence level are outlined by *bold curves*. The numerals superimposed on the curves denote the lag in days toward the past. The *broken curves* are used every 60 days for ease of reference. *Shading* indicates the area in which numbers of Argo floats are counted in Fig. 11

be noted that Argo float numbers drastically change with each forecast run. In fact, numbers in the former three forecast computations (runs 1, 2, and 3) are smaller than those in the latter three computations (runs 4, 5, and 6). In particular, numbers in both runs 5 and 6 are nearly double those in the former three runs.

It is anticipated that eddies that might trigger kyucho events in 2010 appear reliably in the FVCOM domain during the latter three forecast runs because of reliable

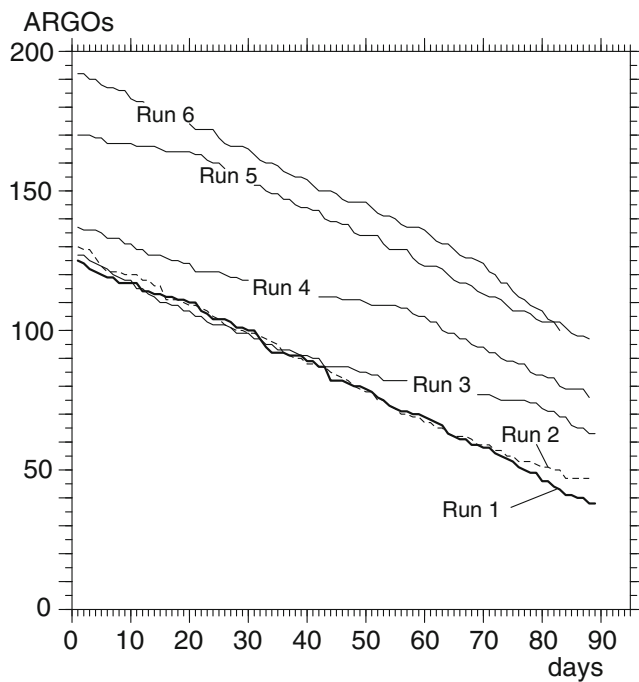


Fig. 11 Number of Argo floats within the shaded area in Fig. 10 in the past 5 months during the 3-month forecast computations. The abscissa indicates elapsed days from the beginning of each forecast run, while the ordinate shows the float number during the past 5 months counted from each day given on the abscissa. The line type and thickness differ among runs 1, 2, and 3 for ease of reference

lateral boundary conditions corrected by numerous Argo data and that the actual kyuchō events are therefore well forecast because of these eddies impinging on the Kuroshio front. We next compare forecast density profiles with density profiles observed by Argo floats south of Japan to examine whether or not the anomalous density field in the forecast computations is consistent with that in the actual ocean. The Argo data during each forecast run are chosen in the area outlined by the broken line in Fig. 4 and are used to compute the anomaly of vertical potential density profile from the profile averaged over the area. Table 1 lists correlation coefficients and skills defined as $1 - \frac{\sum (\sigma_a - \sigma_f)^2}{\sum (\sigma_a - \bar{\sigma}_a)^2}$, where σ is the potential density anomaly above 1,000 m, the overbar indicates the average of all values (i.e., zero in this case), and the subscripts a and f denote densities observed by Argo floats and those computed at the same locations in the forecast runs, respectively. As expected, both correlation coefficients and skills in the latter three forecast runs remain high, while the values fluctuate largely in the former three computations. In fact, in runs 5 and 6 when the number of Argo floats south of Japan in the past 5 months is the largest among all forecast runs (Fig. 11), the sudden temperature rises marked by a , b , and d in Fig. 9 are all forecasted successfully.

Table 1 Comparison of potential density anomalies in the forecast runs and those observed by Argo floats: the number of Argo floats (n) during each forecast run within the box outlined by the broken line in Fig. 4, correlation coefficient (r), and skill (s)

Run	n	r	s
1	47	0.24	-1.26
2	42	0.53	0.20
3	49	0.38	-0.42
4	51	0.71	0.46
5	55	0.51	0.13
6	73	0.51	0.10

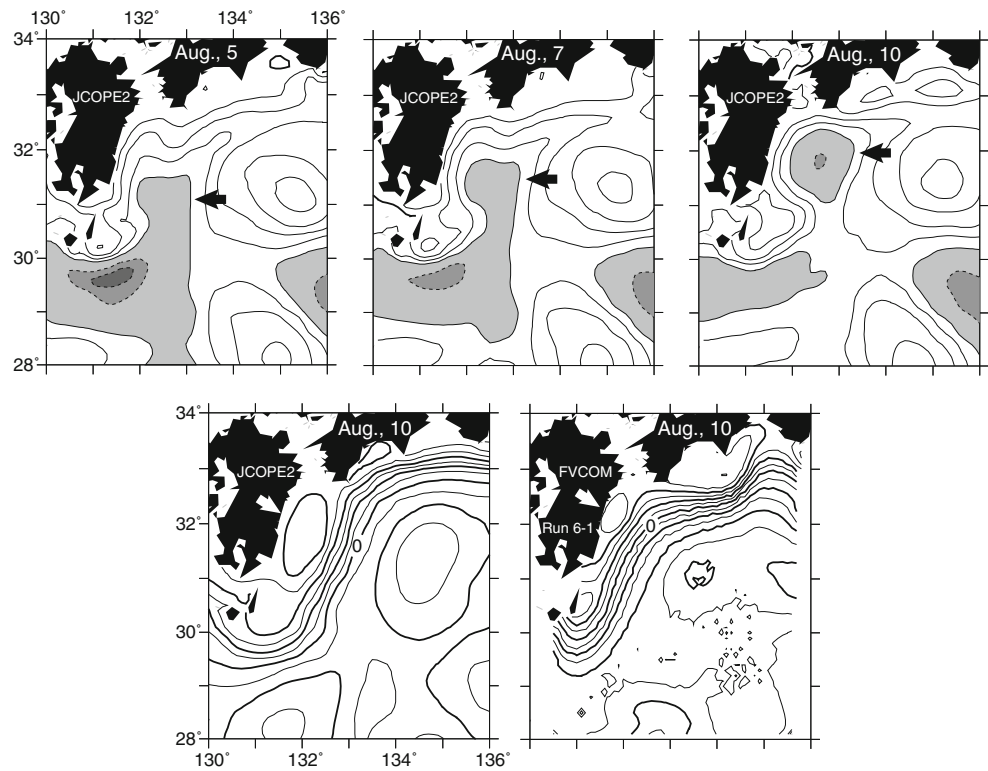
However, Fig. 9 apparently shows that the number of Argo floats is not a unique factor in determining the forecast accuracy. For instance, the sudden temperature rise c in run 6 is not present in the actual time series despite the forecast computation using the lateral boundary conditions corrected by numerous Argo data. Furthermore, the forecast computation goes well in run 1 (Figs. 7 and 9) in spite of there being the least Argo floats among all forecast runs. Hence, factors unrelated to the number of Argo floats south of Japan should be specified to improve this forecast model developed for coastal waters.

4.2 Modeled processes reducing the forecast accuracy

The behavior of relatively small eddies (~100 km) in the FVCOM domain explains why the sudden temperature rise c in run 6 does not exist in the actual time series. In addition to mesoscale eddies impinging on the Kuroshio south of the Bungo Channel, eddies passing through the Tokara Strait (Fig. 1) affect the Kuroshio volume transport south of Japan (Ichikawa 2001). In fact, the SSH anomaly provided by JCOPE2 reanalysis data during run 6 shows that a cold eddy shed from the Tokara Strait moves to the area south of the Bungo Channel; see the arrow in the upper panels in Fig. 12. The cold eddy is located north of the Kuroshio on 10 August 2010 and seems to prevent Kuroshio water from intruding onto the shallow shelf; see the white arrow in the lower left panel of Fig. 12. However, the cold eddy forecast in run 6 is much smaller than that in JCOPE2 reanalysis data (lower right panel). Therefore, the forecast Kuroshio axis is located closer to the channel than that in the reanalysis data, and this is the reason for the kyuchō event (c in Fig. 9) that did not occur in the actual ocean appearing in run 6.

In the case of run 1, a kyuchō-favoring condition is maintained by a warm eddy (the solid circle in the lower panels of Fig. 13) located stably south of Japan during mid-February; see SSH anomaly maps in Fig. 13. In fact, the

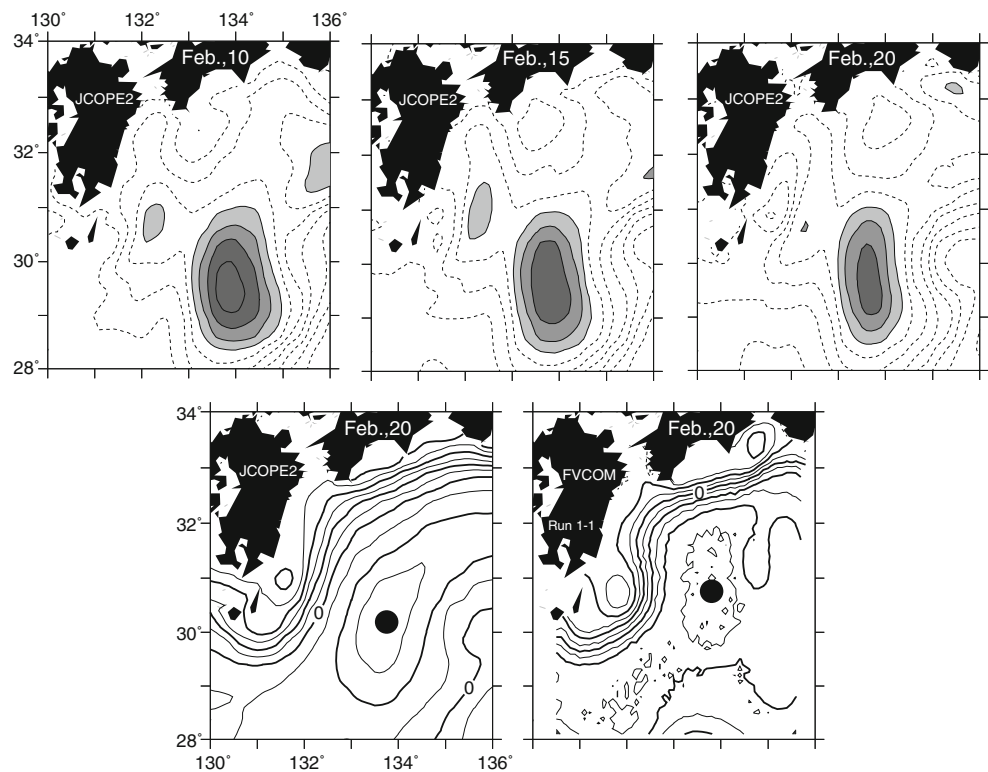
Fig. 12 SSH maps in August. The anomalies from the SSH averaged over the computation period of run 6 are depicted in the upper panels every 5 days using JCOPE2 reanalysis data. Areas with the negative SSH anomalies are indicated by shading. The cold eddy shed from the Tokara Strait is indicated by the arrow. The SSH map using JCOPE2 reanalysis data on 10 August is shown in the lower left panel, while that computed for the first ensemble member of run 6 is depicted in the right panel. In the lower panels, cold eddies located on the onshore side of the Kuroshio are indicated by white arrows. The contour interval in the upper (lower) panel is 5 (10) cm



Kuroshio paths in both JCOPE2 reanalysis data (lower left panel of Fig. 13) and the forecast computation (lower right panel) are located close to the Bungo Channel. Thereby, frontal waves excited along the Kuroshio front extend easily

onto the shelf of the Bungo Channel in both actual and forecast oceans, irrespective of whether or not the SSH distribution except this warm eddy appears reliably in the forecast computation.

Fig. 13 Same as Fig. 12 but for February maps. Unlike Fig. 12, shading in the upper panels represents positive anomalies. The closed circles are plotted in the lower panels for ease of finding the warm eddy south of Japan



5 Conclusion possible improvement of the kyucho forecast model

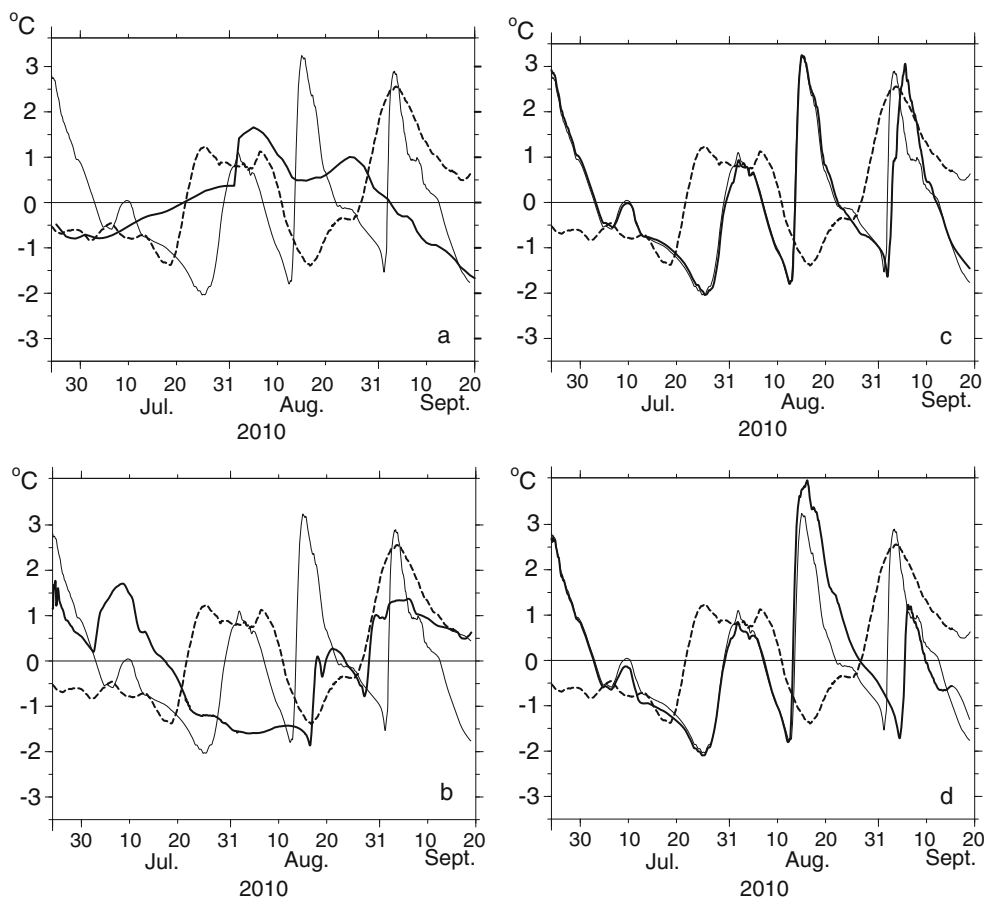
The present study investigated whether numerical models downscaling JCOPE2 reanalysis and forecast data are capable of forecasting ocean circulation in coastal waters. The target oceanic phenomenon in the present study is the kyucho events generated in the Bungo Channel in 2010, when sudden temperature increases caused by Kuroshio water intrusion are observed in February, August, and September. In particular, the Kuroshio front south of the Bungo Channel is favorable for the kyucho occurrence in February because it is located close to the channel owing to the existence of a stable warm eddy south of Japan. This stable eddy is also revealed in the forecast computation (run 1), and the kyucho event thus occurs in the forecast model as in the actual ocean (Figs. 7 and 9). In addition, the kyucho events in August and September (a (b) and d in Fig. 9) are successfully forecasted in the present model, where mesoscale eddies south of Japan appear consistently with those observed as shown by relatively high correlation coefficients and skills during both runs 5 and 6 (Table 1).

The establishment of assimilation methods applicable to coastal waters will enhance the accuracy of hindcast computations (and hence, the initial condition of forecasts). Besides the assimilation methods, the present forecast model has

shortcomings that we should overcome to establish operationally practical kyucho forecast models. In particular, kyucho events that did not occur in the actual ocean often appear in the model (Fig. 9). For instance, the forecast kyucho event in mid-August (c in Fig. 9) is prevented from forming in the actual ocean by the cold eddy moving along the shelf break (Fig. 12). Apparently, this cold eddy is advected by the Kuroshio along the shelf break south of the Bungo Channel, and it is thus considered that short-term fluctuations in the current speed cause the detachment of the eddy in mid-August. If this is the case, the suggestion is that the daily wind forcing and/or tidal currents at the shelf break, which are omitted in the present model, are required to enhance the forecast accuracy.

The above arguments are also supported by extra experiments carried out to examine the dependency of the forecast accuracy on the model design. Figure 14 shows the same time series of temperature at 5-m depth as those in run 6 in Fig. 9, except for the first ensemble member (i.e., runs 6–1). Run 6 is chosen for the experiments because the number of Argo floats was the largest among all forecast runs (Fig. 11) and because the model accuracy is insensitive to the lateral boundary conditions. Also shown by the bold lines in Fig. 14 are (a) the time series obtained at the same location in the JCOPE2 analysis, (b) the time series obtained by the computation using daily wind stresses instead of monthly wind stresses, (c) time series

Fig. 14 Temperature time series in extra experiments. The thin and broken curves represent the same quantities as those of run 6 in Fig. 9, but for the first ensemble member (i.e., runs 6–1). The bold curves in a to d represent the time series in extra experiments; see the text for details



obtained by the computation in which the time scale taken to restore SST in the FVCOM domain to the monthly average is doubled (i.e., 10 days), and (d) the time series obtained by the computation in which the standard deviation of initial perturbations added to each forecast run is doubled (i.e., 0.2°C). The forecast daily winds are not used in computing wind stresses with the drag coefficients of Large and Pond (1981), but those observed by ASCAT (Kako et al. 2011) are used in this experiment. That is to say, the present application provides us with results using the wind stresses that are forecasted “perfectly”. Figure 14a indicates that the downscaling to the FVCOM domain is effective in reproducing kyucho events because the temperature fluctuations with periods shorter than 1 month are not revealed in the relatively coarse JCOPE2 analysis. It is noted that these short-term fluctuations are sensitive to the daily wind stresses (b) in comparison with both the restoring time of SST (c) and magnitude of initial perturbations (d). It is likely that accurately forecasted wind stresses with fine resolution are required to forecast kyucho events in coastal waters under the complex orographic conditions and that these winds (and/or tidal currents) might be required to forecast the behavior of small-scale eddies like those in Fig. 12.

Kyucho events accompanied by large temperature rises are frequently forecasted during the period May through June when intense kyucho events are absent in the actual ocean (Fig. 9). The forecast computations during this period are conducted using lateral boundary conditions that pass through areas with less Argo data. In fact, runs 5 and 6 using lateral boundary conditions, which undergo assimilating numerous Argo data, result in relatively high and stable correlation coefficients and skills between forecast and reanalysis density profiles and successfully forecast the kyucho events actually observed in August and September. The suggestion is that one of the most efficient improvements in forecasting coastal waters is to deploy numerous Argo floats offshore, but this improvement is beyond a scientific issue.

Acknowledgments Professor Lie-Yauw Oey and all other members of the scientific committee provided the authors with the opportunity to present this topic at the 3rd International Workshop of Modeling the Ocean (IWMO-2011), which we greatly appreciated. Comments of two anonymous reviewers are very helpful in improving the manuscript and are appreciated. This work is supported by the Japan Society for the Promotion of Science KAKENHI (21244073).

Open Access This article is distributed under the terms of the Creative Commons Attribution Noncommercial License which permits any noncommercial use, distribution, and reproduction in any medium, provided the original author(s) and source are credited.

References

- Akiyama H, Saitoh S (1993) The kyucho in Sukumo Bay induced by Kuroshio warm filament intrusion. *J Oceanogr* 49:667–682
- Arai M (2005) Numerical study of a kyucho and bottom intrusion in the Bungo Channel, Japan: disturbances generated by the Kuroshio small meanders. *J Oceanogr* 61:953–971
- Chang P-H, Guo X, Takeoka H (2009) A numerical study of the seasonal circulation in the Seto Inland Sea. *Japan J Oceanogr* 65:721–736
- Chen C, Liu H, Beardsley RC (2003) An unstructured grid, finite-volume, three-dimensional, primitive equations ocean model: application to coastal ocean and estuaries. *J Atmos Oceanic Technol* 20:159–186
- Hirose M, Katano T, Hayami Y, Kaneda A, Kohama T, Takeoka H, Nakano S (2008) Changes in the abundance and composition of picophytoplankton in relation to the occurrence of a kyucho and a bottom intrusion in the Bungo Channel, Japan. *Estuarine Coastal Mar Sci* 76:293–303
- Ichikawa K (2001) Variation of the Kuroshio in the Tokara Strait induced by meso-scale eddies. *J Oceanogr* 57:55–68
- Isobe A, Fujiwara E, Chang PH, Sugimatsu K, Shimizu M, Matsuno T, Manda A (2004) Intrusion of less saline shelf water into the Kuroshio subsurface layer in the East China Sea. *J Oceanogr* 60:853–863
- Isobe A, Guo X, Takeoka H (2010) Hindcast and predictability of sporadic Kuroshio-water intrusion (kyucho in the Bungo Channel) into the shelf and coastal waters. *J Geophys Res* 115:C04023. doi:10.1029/2009JC005818
- James C, Wimbush M, Ichikawa H (1999) Kuroshio meanders in the East China Sea. *J Phys Oceanogr* 29:259–272
- Kako S, Isobe A, Kubota M (2011) High-resolution ASCAT wind vector dataset gridded by applying an optimum interpolation method to the global ocean. *J Geophys Res* 116:D23107. doi:10.1029/2010JD015484
- Katano T et al (2007) Distribution of prokaryotic picophytoplankton from Seto Inland Sea to the Kuroshio region, with special reference to ‘kyucho’ events. *Aquat Microb Ecol* 46:191–201
- Koizumi Y, Kohno Y (1994) An influence of the kyucho on a mechanism of diatom growth in Shitaba Bay in summer. *Bull Coastal Oceanogr* 32:81–89 (in Japanese with English abstract)
- Large WG, Pond S (1981) Open ocean momentum flux measurements in moderate to strong winds. *J Phys Oceanogr* 11:324–336
- Masumoto Y et al (2004) A fifty-year eddy-resolving simulation of the world ocean—preliminary outcomes of OFES (OGCM for the Earth Simulator). *J Earth Sim* 1:35–56
- Miyazawa Y, Yamane S, Guo X, Yamagata T (2005) Ensemble forecast of the Kuroshio meandering. *J Geophys Res* 110:C10026. doi:10.1029/2004JC002426
- Miyazawa Y, Kagimoto T, Guo X, Sakuma H (2008) The Kuroshio large meander formation in 2004 analyzed by an eddy-resolving ocean forecast system. *J Geophys Res* 113:C10015. doi:10.1029/2007JC004226
- Miyazawa Y, Zhang R, Guo X, Tamura H, Ambe D, Lee JS, Okuno A, Yoshinari H, Setou T, Komatsu K (2009) Water mass variability in the western North Pacific detected in a 15-year eddy resolving ocean reanalysis. *J Oceanogr* 65:737–756
- Oka E, Talley LD, Suga T (2007) Temporal variability of winter mixed layer in the mid- to high-latitude North Pacific. *J Oceanogr* 63:293–307
- Takeoka H, Yoshimura T (1988) The kyucho in Uwajima Bay. *J Oceanogr Soc Japan* 44:6–16
- Takeoka H, Akiyama H, Kikuchi T (1993) The kyucho in the Bungo Channel, Japan—periodic intrusion of oceanic warm water. *J Oceanogr* 49:369–382
- Toth Z, Kalnay E (1993) Ensemble forecasting at NMC: the generation of perturbations. *Bull Am Meteorol Soc* 74:2317–2330
- Uda M (1953) On the stormy current (Kyutyo) and its prediction in the Sagami Bay. *J Oceanogr Soc Japan* 9:15–22 (in Japanese with English abstract)